JUN 9 1982

Y 3. N88 : 25/2633

NUREG/CR-2633
LA-9277-MS

Containment Reactor Cavity Subcompartment Analysis Procedures for a Boiling Water Reactor

COMPLETED

ORIGINAL

Prepared by W. V. Turk, R. G. Gido, C. Y. Li

Los Alamos National Laboratory

Prepared for
U.S. Nuclear Regulatory
Commission

33

NOTICE

This report was prepared as an account of work sponsored by an agency of the United States Government. Neither the United States Government nor any agency thereof, or any of their employees, makes any warranty, expressed or implied, or assumes any legal liability of responsibility for any third party's use, or the results of such use, of any information, apparatus, product or process disclosed in this report, or represents that its use by such third party would not infringe privately owned rights.

Availability of Reference Materials Cited in NRC Publications

Most documents cited in NRC publications will be available from one of the following sources:

1. The NRC Public Document Room, 1717 H Street, N.W.
   Washington, DC 20555
2. The NRC/GPO Sales Program, U.S. Nuclear Regulatory Commission,
   Washington, DC 20555
3. The National Technical Information Service, Springfield, VA 22161

Although the listing that follows represents the majority of documents cited in NRC publications, it is not intended to be exhaustive.

Referenced documents available for inspection and copying for a fee from the NRC Public Document Room include NRC correspondence and internal NRC memoranda; NRC Office of Inspection and Enforcement bulletins, circulars, information notices, inspection and investigation notices; Licensee Event Reports; vendor reports and correspondence; Commission papers; and applicant and licensee documents and correspondence.

The following documents in the NUREG series are available for purchase from the NRC/GPO Sales Program: formal NRC staff and contractor reports, NRC-sponsored conference proceedings, and NRC booklets and brochures. Also available are Regulatory Guides, NRC regulations in the *Code of Federal Regulations,* and *Nuclear Regulatory Commission Issuances.*

Documents available from the National Technical Information Service include NUREG series reports and technical reports prepared by other federal agencies and reports prepared by the Atomic Energy Commission, forerunner agency to the Nuclear Regulatory Commission.

Documents available from public and special technical libraries include all open literature items, such as books, journal and periodical articles, and transactions. *Federal Register* notices, federal and state legislation, and congressional reports can usually be obtained from these libraries.

Documents such as theses, dissertations, foreign reports and translations, and non-NRC conference proceedings are available for purchase from the organization sponsoring the publication cited.

Single copies of NRC draft reports are available free upon written request to the Division of Technical Information and Document Control, U.S. Nuclear Regulatory Commission, Washington, DC 20555.

Copies of industry codes and standards used in a substantive manner in the NRC regulatory process are maintained at the NRC Library, 7920 Norfolk Avenue, Bethesda, Maryland, and are available there for reference use by the public. Codes and standards are usually copyrighted and may be purchased from the originating organization or, if they are American National Standards, from the American National Standards Institute, 1430 Broadway, New York, NY 10018.

GPO Printed copy price: $2.75

Affirmative Action/Equal Opportunity Employer

NUREG/CR-2633
LA-9277-MS

Containment Reactor Cavity Subcompartment Analysis Procedures for a Boiling Water Reactor

Manuscript Completed: February 1982
Date Published: May 1982

Prepared by
W. V. Turk, R. G. Gido, C. Y. Li*

Los Alamos National Laboratory
Los Alamos, NM 87545

*Staff, U.S. Nuclear Regulatory Commission

Prepared for
Division of Systems Integration
Office of Nuclear Reactor Regulation
U.S. Nuclear Regulatory Commission
Washington, D.C. 20555
NRC FIN A7119

TABLE OF CONTENTS

		Page
ABSTRACT		1
I.	PURPOSE	1
II.	THE PROBLEM	2
III.	APPROACH	3
IV.	PROCEDURES	4
	A. Noding	5
	1. General Procedure for Noding	5
	2. Effects of Consolidation	8
	3. Different Reactor Cavities	8
	B. Heat Transfer	9
	C. Blowdown	9
	D. Initial Conditions	10
	E. Flow Modeling	10
	1. Air Accounting	10
	2. Inertial Representation	10
	3. Compressibility	11
	4. Critical Flow Models	11
	F. Flow Area	11
	G. Loss Coefficients	12
	1. Sources	12
	2. Flow Direction Effect	12
	3. Area Ratio Multiplier	12
	4. Node-to-Junction Representation	12
	5. Compressibility	12
	6. Detailing of Junction Loss-Coefficient Components	12
	H. Force-Moment Determination	13
	1. General	13
	2. Nozzle and Piping Considerations	13
REFERENCES		13
APPENDIX A.	APPLICATION OF GENERAL NODING PROCEDURES TO REPRESENTATIVE BWR CAVITY	14
APPENDIX B.	EFFECT OF BWR CAVITY NODE CONSOLIDATION ON SACRIFICIAL SHIELD-WALL FORCES AND MOMENTS	16
APPENDIX C.	EFFECT OF NODE CONSOLIDATION FOR OTHER BWR CAVITY GEOMETRIES	19
APPENDIX D.	SENSITIVITY STUDIES	23

LIST OF TABLES

A-I	Description of SSW Pipe Penetrations Shown in Fig. A-1	16
B-I	Effect of Node Consolidation on BWR SSW Maximum Force (F_x) and Moment (M_y)	17
C-I	Effect of Node Consolidation on Maximum SSW Forces and Moments for Different Annulus Widths	20
C-II	Effect of Node Consolidation on Maximum SSW Forces and Moments for Different Numbers of Feedwater Pipes	20
C-III	Effect of Changing Break-Node Outflow Area Ratio	21
C-IV	Mass-Flow Rate and Mass-Flow Ratios as a Function of Time	22

LIST OF TABLES (Cont.)

		Page
D-I	Effect of Critical Flow Model and Noding on SSW Loads.	23
D-II	Effects on Forces and Moments on Varying Inertia Terms	24
D-III	Effects on Forces and Moments of Varying Entrance and Exit Loss. . .	24

LIST OF FIGURES

		Page
1a.	BWR cavity x-z cross section showing drywell, SSW, break in SSW, annulus between insulation and SSW, reactor pressure vessel, and stabilizer around which flow exists from the annulus.	2
1b.	Illustration of SSW showing coordinate system. Note that the y-moment discussed in this report is taken about the SSW bottom. Other SSW penetrations are not shown for clarity. . . .	2
1c.	Detail showing break location in SSW, break node, flow area from break node to annulus between SSW and insulation, and flow area from break node to drywell	3
2.	Noding of the BWR cavity described in Fig. 3 based upon the procedures described in Sec. IV.A.1. Note that in the computer model, a few pipes were shifted slightly so that their new location corresponded to a nearby intersection of a horizontal and a vertical junction row.	6
3.	This is the "unwrapped" BWR reactor cavity that was studied showing pipe locations in the symmetric 0 to π rad model used for calculations. Also shown is the elevation from the SSW bottom ($z = 0$) and the annulus gap (between the SSW and insulation) variation.	6
4.	Illustrations showing good and poor methods of locating the break. .	7
5.	Top view of reactor cavity showing good break locations (●).	7
6.	Examples of good and poor location of junctions to account for pressure differences at $\pi/2$ rad (90°) for a symmetric model with the force direction of importance going through 0 and π rad.	7
7.	Examples of poor and good junction locations for a symmetric model with the force direction of importance going through 0 and π rad.	7
8.	Example of good junction location (▯) for a 0 to 2π rad model with x-force being important	8
9.	Illustrations showing good and poor placement of junctions over openings in the SSW.	8
10.	Illustrations of good and poor methods of placing junctions on a stepped annulus reactor cavity. Fig. 10b shows a row of junctions placed on the step in the annulus.	8
11.	Illustrations of good and poor methods of treating large featureless areas of annulus. Junctions should be placed on these areas	9

LIST OF FIGURES (Cont.)

		Page
12.	Acceptable consolidation (42 annulus nodes).	9
13.	Graphic representation showing three nodes of different coarseness and derivation of L/A terms	11
A-1.	This is the "unwrapped" BWR cavity that was studied in this report showing pipe (see Table A-I) locations in the symmetric 0 to π rad model used for calculations. Also shown are the elevation from the SSW bottom ($z = 0$) and the annulus gap (between the SSW and insulation) variation. Blowdown is introduced at the recirculation outlet pipe located at 0 rad and $z \cong 5$ m (~ 16 ft.). There is exit flow from the annulus top around the stabilizers and through the SSW penetrations associated with the core spray (7) and the feedwater pipes (8) . . .	15
A-2.	Noding of the BWR cavity described in Fig. A-1 based upon the procedures described in Sec. IV.A.1	15
B-1.	Progressive consolidated noding of the base-case noding shown in Fig. A-2 with 72 annulus nodes. See Table B-I for the effect of noding consolidation on SSW loading. Note that Case 5 is the "acceptable" consolidation noding used in other studies in this report.	17

Blank Page

CONTAINMENT REACTOR CAVITY SUBCOMPARTMENT ANALYSIS PROCEDURES FOR A BOILING WATER REACTOR

by

W. V. Turk, R. G. Gido, and C. Y. Li

ABSTRACT

Procedures for the performance of Boiling Water Reactor (BWR) cavity subcompartment analysis are presented. The purpose of this presentation is to normalize the analysis procedures and to provide a standard approach for such analyses. As a result, differences in the manner of performing subcompartment analyses can be minimized and more readily understood and evaluated by others. The procedures were developed within the constraint of current code capability for the performance of such analyses and the current US Nuclear Regulatory Commission guidelines. A wide range of the effects of input and modeling variations on calculated sacrificial shield-wall (SSW) forces and moments were studied. The studies were for a representative BWR cavity geometry with the pipe break inside the SSW. The COMPARE subcompartment analysis code was used for the studies.

I. PURPOSE

The purpose of this report is to develop standard modeling procedures for the performance of Boiling Water Reactor (BWR) cavity subcompartment analysis. Reference 1 presents a similar development for Pressurized Water Reactor (PWR) cavities. Such standardization will significantly improve the efficiency of subcompartment-analysis model development and the subsequent acceptance of the models by others. The standardization is necessarily constrained by (1) guidelines of the US Nuclear Regulatory Commission (NRC) Standard Review Plan[2] and (2) computer codes that are currently available (for example, Refs. 3, 4, and 5).

A subcompartment is any fully or partially enclosed volume within the nuclear power plant containment that is influenced by the pressure developed because of a postulated high-energy line break. A good example is the reactor cavity. The break introduces mass and energy blowdown addition into the subcompartment geometry that results in pressure, force, and moment loads on walls and components. Analytical flow models account for the break mass and energy-flow distribution throughout the subcompartment and adjacent regions.

Subcompartment loads may be significantly affected by the analytical modeling procedures, which vary between modelers. In addition, unnecessary complexity may produce small changes in calculated results. This report attempts to normalize these subcompartment analysis procedures so that models can be developed in a more direct and efficient manner than has been previously available. The application of these procedures should minimize the differences between modeling approaches.

Our primary basis for the establishment of these procedures has been sensitivity studies using a representative BWR cavity with the pipe

break in the sacrificial shield wall (SSW). These studies were simply a matter of varying the modeling procedures to see how the SSW loads were affected. A word of caution is, therefore, necessary. Because the sensitivity studies used are those for a reactor cavity, application of the procedures to other subcompartments must be done cautiously. This is because of the different geometries and blowdowns that may be associated with different subcompartments. Similarly, caution should be used for reactor cavity subcompartments that are significantly different from those studied.

Certain sensitivity studies performed in the PWR study[1] were not performed in the BWR study because we believed that the PWR results would be applicable. In fact, it is recommended that the PWR and BWR studies be used together because they complement each other.

II. THE PROBLEM

The reactor cavity region represents the major area for subcompartment analysis; however, other subcompartments also require analysis. Reactor-cavity subcompartment analyses include all of the geometric and flow situations to be found.

For a reactor-cavity subcompartment analysis, breaks are postulated to occur in the pipes attached to the pressure vessel. The water mass and energy released from the break generate pressure waves that propagate throughout the reactor-cavity region. Pressure differences across components and shield wall are developed and force and moment loads result. The maximum loads usually occur in less than 1 s and are ultimately relieved by the distribution of flow to the major containment volume.

We have analyzed the BWR cavity depicted in Figs. 1a - 1c, which is characterized by the break being located in the SSW. Note that the orthogonal coordinate system used has its origin at the bottom of the SSW with its x-axis going through the angular location of the broken pipe (see Fig. 1b). Several other BWR cavities of similar geometry were found to have only minor differences, such as the number of auxiliary

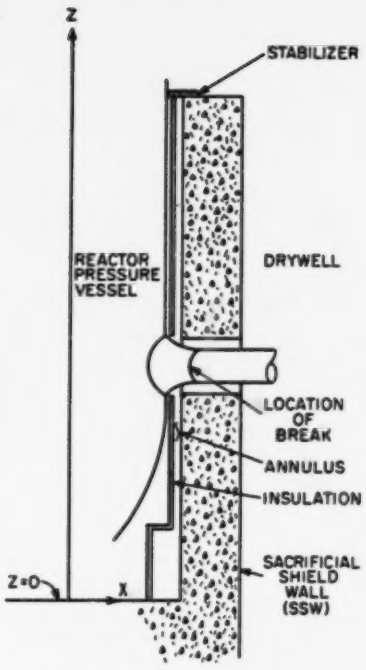

Fig. 1a. BWR cavity x-z cross section showing drywell, SSW, break in SSW, annulus between insulation and SSW, reactor pressure vessel, and stabilizer around which flow exists from the annulus.

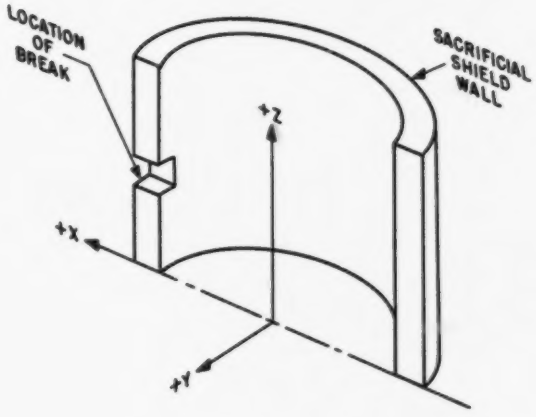

Fig. 1b. Illustration of SSW showing coordinate system. Note that the y-moment discussed in this report is taken about the SSW bottom. Other SSW penetrations are not shown for clarity.

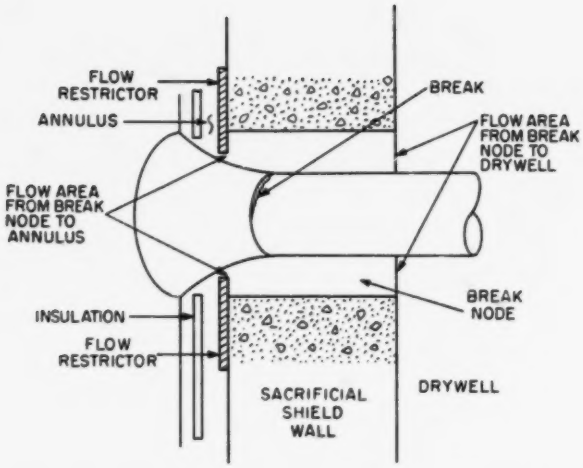

Fig. 1c. Detail showing break location in SSW, break node, flow area from break node to annulus between SSW and insulation, and flow area from break node to drywell.

feedwater pipes and the thickness of the annulus between the SSW and the insulation. The effects of these differences on SSW loads were studied as one part of the sensitivity studies. Note that some BWR cavity geometries, such as the General Electric Mark III, are very different than the geometry studied.

The results of the sensitivity studies that we performed are presented in the appendixes. These studies have emphasized the effect of noding and basic input-parameter variations on maximum calculated SSW forces and moments. All of the calculated results had similar variation with time of the SSW forces and moments.

III. APPROACH

Any development of subcompartment-analysis procedures is somewhat constrained by the engineering analysis tools currently available for subcompartment analysis. These tools are characterized by the COMPARE subcompartment-analysis computer code, which was used in the studies of this report.[3,4] Advanced codes (for example, BEACON[6]) are under development and will be used in the future to evaluate the importance of simplifying assumptions utilized in current codes.

The currently available analytical tools for subcompartment analysis incorporate several relatively fixed general features that may strongly influence modeling procedures. It is important to identify and understand these features. This is particularly true because the procedural discussions below are often relative to these features. The features are

(1) one-dimensional flow equations - As a result, large two-dimensional flows must be represented by nodes (subvolumes) connected by one-dimensional flow paths;

(2) lumped nodal representation - Mean thermodynamic properties, such as pressure and temperature, are determined in the nodes. As a result, pressure distributions are represented by mean values. Total pressure is used instead of the more correct static pressure plus some fraction of the dynamic head;

(3) junctions between nodes - Flow between nodes is based on junction-flow models that account for flow resistance caused by friction, flow losses (such as expansion and contraction), and inertia. Junction locations are clearly called for by the geometric definition of major resistances to flow, such as changes in flow area. Junctions in constant-area flow passages may also be necessary to provide resolution of density and inertia details. Flow limitation caused by the occurrence of critical flow can only be achieved at junctions;

(4) critical flow - The flow rate at a flow junction is limited to the critical value corresponding to the upstream thermodynamic conditions, the junction minimum flow area, and possibly flow losses. There is no provision for the modeling of shocks or supersonic flow;

(5) compressibility effects - Compressibility effects are treated to a limited extent. For example, a one-dimensional, constant-density, momentum equation is used in the COMPARE code[3,4] with the density value based on compressibility considerations. Compressibility may also affect loss coefficients;

(6) loss coefficients and friction factors - Conventional, single-phase, incompressible loss coefficients and friction factors are currently used. The effects of compressibility and loss

coefficients are discussed below in Secs. IV.E.3 and IV.G.5, respectively. These discussions indicate that the effects of compressibility on loss coefficients are small and that the effects of loss coefficients are, in turn, small. As a result, the assumption of incompressibility appears quite acceptable. On the other hand, the effects of compressibility on loss coefficients have been studied and could be readily incorporated into the calculational procedures;

(7) inertia term (L/A) - Fluid inertia is represented by an integrated flow-path length/area (L/A) term that evolves from the solution of the one-dimensional flow equations with constant density assumed;

(8) entrainment - A homogeneous mixture in thermal equilibrium with 100 per cent liquid water entrainment is used because (a) it conforms to the Ref. 2 NRC guideline for subcompartment analysis; (b) it will result in higher calculated pressures near the break, which will usually result in higher calculated forces and moments; and (c) 100 per cent liquid water entrainment has been shown to be a good approximation (see Ref. 7).

This discussion points out that the performance of subcompartment analysis involves many assumptions. The assumptions above are currently used in the COMPARE code and, to some degree, in other codes. Therefore, the procedures for performing analyses were based on COMPARE. However, the use of different codes may require recognition of code-specific characteristics; in addition, the influence of these characteristics may depend on the subcompartment analyzed. Therefore, it may be prudent to perform sensitivity studies to ensure that desired results, for example, maximum loads, are obtained.

We have used the results of sensitivity studies (see appendixes) to develop the procedures outlined in Sec. IV. These studies investigated the effect of input parameter variations on subcompartment loads. It was decided to use the maximum calculated SSW forces and moments as a measure of the effects of the variations in order to facilitate the comparisons of the loading transients. For example, this approach will not be totally valid when a load that is not necessarily the maximum at a particular time is important.

IV. PROCEDURES

Procedures for subcompartment-analysis modeling are discussed in this section to standardize model development. This is not possible for all the modeling considerations discussed because of the uniqueness of (1) the codes used, (2) the subcompartment geometry, and/or (3) the calculated result desired. For these unique situations, parameters may require variation to determine the appropriate model input.

An obvious prerequisite for any subcompartment analysis is a complete representation of the geometry to be analyzed. Because the analysis pertains to the calculation of pressure in a system of volumes connected by flow paths, geometric details that would influence such calculation are important. Such details include the following: changes in flow area (for example, change in annulus width); flow restrictions (for example, pipes, neutron detectors); movable vent closures (for example, seals); and vent plugging (for example, because of insulation). Establishment of the analytical model details, including noding, would then result in a schematic representation of the physical geometry in nodal (subvolume) form. It is easier to understand both the original model and any modifications needed to incorporate new information if the subcompartment geometry and its corresponding model are thoroughly represented.

The discussion that follows includes the same value judgments regarding the importance of modeling procedures as were used in the PWR study.[1] The judgments are based on sensitivity studies that show the effect of modeling variations on the SSW loads of BWR cavities. To quantify the value judgements, the following arbitrary equivalences will be used.

Verbal Equivalence	% Effect
Insensitive	0 - 5
Sensitive	5 - 20
Very Sensitive	Greater than 20

A. Noding

Noding is the process of dividing the subcompartment into nodes (that is, cells or subvolumes) for calculational purposes. This is a conventional procedure for numerical analysis (for example, finite difference conduction analysis). A characteristic of noding is that calculated results should not change significantly after a certain fineness of noding size is obtained. That is, the averaging and lumping effects become as complete as practical, and further refinement only adds to the model details and computer running time. Ideally, a good noding procedure results in a sufficiently fine noding to produce results that change little with increased refinement.

Before noding can begin, some general procedures are needed to provide a general accounting for geometric features that might affect the flow distribution; this is done in Sec. IV.A.1. Application of these general procedures in Appendix A results in the detailed base-case noding diagram shown in Figs. 2 and A-2. Starting with this base-case noding, Appendix B investigates the effect of node consolidation on SSW loads; this is discussed in Sec. IV.A.2 below.

The noding studies, and all other sensitivity studies of this report, relate to the basic geometry depicted by Figs. 1a - 1c with the piping arrangement and annulus thickness described by Fig. 3. However, there are BWR cavities with similar basic geometries that have a smaller annulus thickness and fewer auxiliary feedwater pipes. The effect of node consolidation on SSW loads for these slightly different geometries is discussed in Sec. IV.A.3. Note that there are BWR cavity geometries, such as the General Electric Mark III, that are very different from the geometry studied.

1. General Procedure for Noding. To make the task of subcompartment analysis easier, we have developed some general procedures to assist in creating the noding for most reactor cavities based on Ref. 1. They are presented below. Appendix A shows how these rules can be applied. Figure 2 is the resulting noding diagram. Note that in Fig. 2, junctions are depicted by a dashed line (that is, -- -- --), whereas in the following diagrams, the junctions are represented by a lightface solid line (that is, ——————). The diagrams that follow show the "unwrapped" reactor-cavity annulus noding diagram with a horizontal coordinate of angle and a vertical coordinate of height. The angle is measured from the +x axis.

Most reactor-cavity problems are symmetrical around the reactor cavity. Therefore, one may need to model only one-half of the circumference. In this case, the centerline of the break should be placed at 0π rad (0°) or π rad (180°) as shown in Figs. 4 and 5.

It should be noted that some situations may require complete modeling of the entire 2π rad (360°) circumference. For example, an asymmetrical pipe penetration arrangement would require 2π modeling. The procedure that we have just presented would not be applicable in this case. However, all of the procedures that follow would apply to a π rad (180°) and a 2π rad (360°) model.

To obtain good force-moment results, a row of junctions should be placed at an angle of π/2 (90°) from the direction of any force vector of interest that is the result of pressure differences around the circumference of the reactor cavity. This recommendation is made to account for pressure differences that might exist across the plane normal to the force vector. If there were no junctions as recommended, no pressure differences would be calculated and no force component in the direction of interest could be calculated. However, if for some reason junctions cannot be placed at exactly the π/2 rad from the break location, junctions should be placed as close as possible to the π/2 rad from the break location.

Examples of the application of the above procedure include (1) a symmetrical (0 to π rad) model with the break on the x-axis and with the x-force being important should have a row of junctions at the y-axis as shown in Figs. 6, 7, and 8 (2) a 0 to 2π rad model with the break on the x-axis and with the x-force being important should have a row of junctions at the + and the

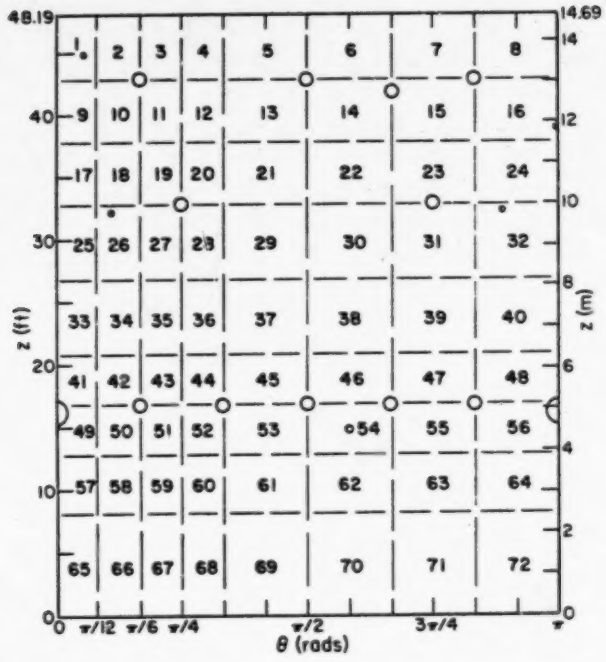

Fig. 2. Noding of the BWR cavity described in Fig. 3 based upon the procedures described in Sec. IV.A.1. Note that in the computer model, a few pipes were shifted slightly so that their new location corresponded to a nearby intersection of a horizontal and a vertical junction row. This figure is also shown as Fig. A-2 in Appendix A.

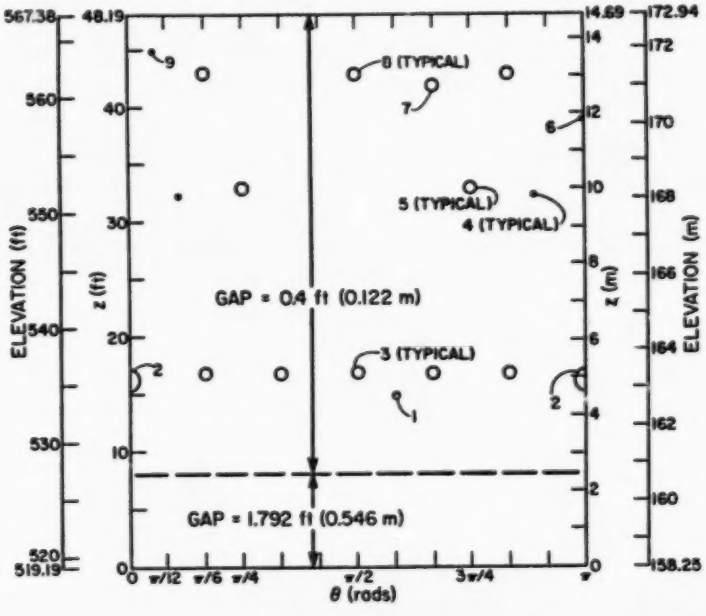

Fig. 3. This is the "unwrapped" BWR cavity that was studied showing pipe locations in the symmetric 0 to π rad model used for calculations. Also shown is the elevation from the SSW bottom (z = 0) and the annulus gap (between the SSW and insulation) variation. This figure is also shown in Appendix A as Fig. A-1.

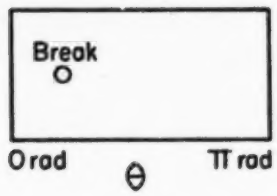

a. Poor

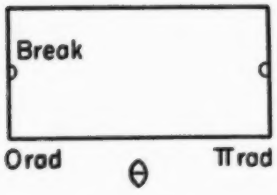

b. Good

Fig. 4. Illustrations showing good and poor methods of locating the break.

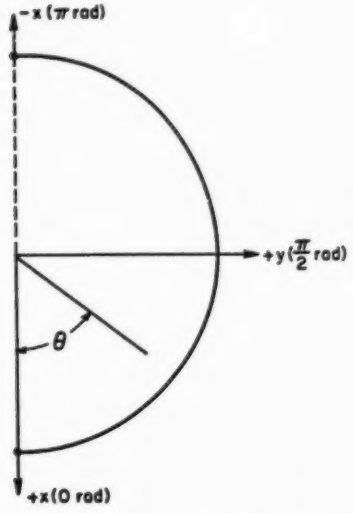

Fig. 5. Top view of reactor cavity showing good break locations (●).

-y-axes, and (3) a 0 to 2π rad model with the break located between the +x-axis and the +y-axis, and with the force direction of importance going through the break location and the common point of the x- and the y-axes, should have a row of junctions between the +y-axis and the -x-axis and a row of junctions between the +x-axis and the -y-axis.

Openings in the SSW may cause significant pressure differences. Obstructions, such as

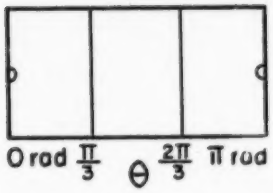

a. Poor

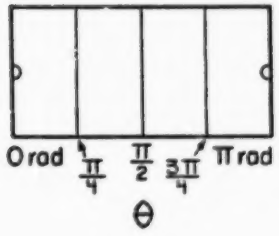

b. Good

Fig. 6. Examples of good and poor location of junctions to account for pressure differences at π/2 rad (90°) for a symmetric model with the force direction of importance going through 0 and π rad.

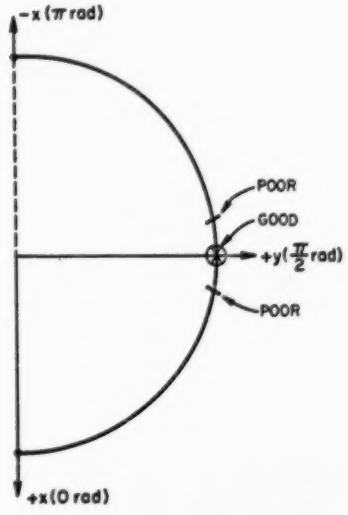

Fig. 7. Examples of poor and good junction locations for a symmetric model with the force direction of importance going through 0 and π rad.

pipes, and the reactor vessel stablizers at the top of the SSW also produce pressure differences and flow restrictions. To correctly model the mass flows, forces, and flow restrictions near

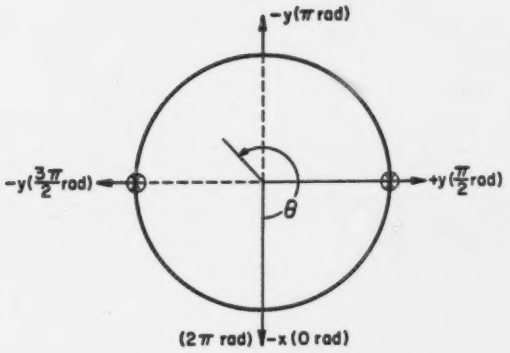

Fig. 8. Example of good junction location (θ) for a 0 to 2π rad model with x-force being important.

these features, junctions should be placed on all major obstructions and openings in the SSW. Figure 9 shows good placement of junctions.

Changes in the width of the annulus induce flow restrictions, and therefore, should have junctions as shown in Fig. 10. The heavy solid line on the "unwrapped" noding diagram represents the location of the step change in annulus thickness.

Large areas of constant annulus width with no geometric features that result in flow area changes should also have junctions, although the spacing and placement of these junctions is a matter of personal discretion. These junctions may be extensions of existing junction strings (see Fig. 11).

2. Effects of Consolidation. Appendix B investigates the effect of noding consolidations on maximum SSW loads. The base-case noding used as a starting point is that developed in Appendix A from the application of the general noding procedures described in Sec. IV.A.1 above. Figure A-2 shows the resulting base-case noding.

In Appendix B, nodes are progressively consolidated with nodes farthest from the break consolidated first. It was found that the calculated maximum loads, their time of occurrence, and their variation with time were approximately insensitive to extensive consolidation. For example, the noding depicted in Fig. 12 (Case 5), with 42 annular nodes, had maximum loads less than 7 per cent different from that for the base case with 72 annular nodes. An interesting result

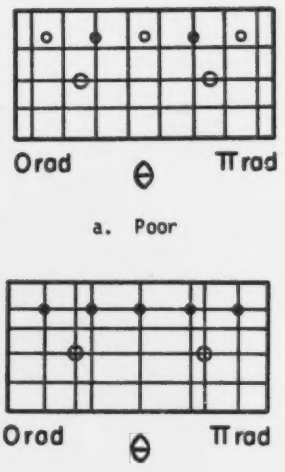

Fig. 9. Illustrations showing good and poor placement of junctions over openings in the SSW.

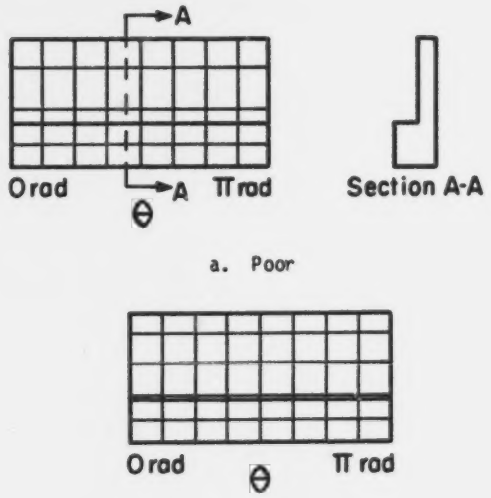

Fig. 10. Illustrations of good and poor methods of placing junctions on a stepped annulus reactor cavity. Fig. 10b shows a row of junctions placed on the step in the annulus.

of further consolidation was that extensive additional consolidation was possible with the resulting loads being less than 11 per cent different from the base case values.

3. Different Reactor Cavities. The basic geometry of BWR cavities is shown in Figs. 1a - 1c

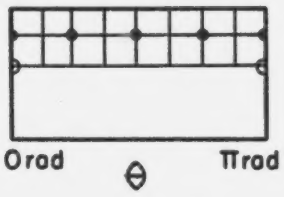

a. Poor

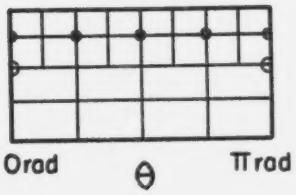

b. Good

Fig. 11. Illustrations of good and poor methods of treating large featureless areas of annulus. Junctions should be placed on these areas.

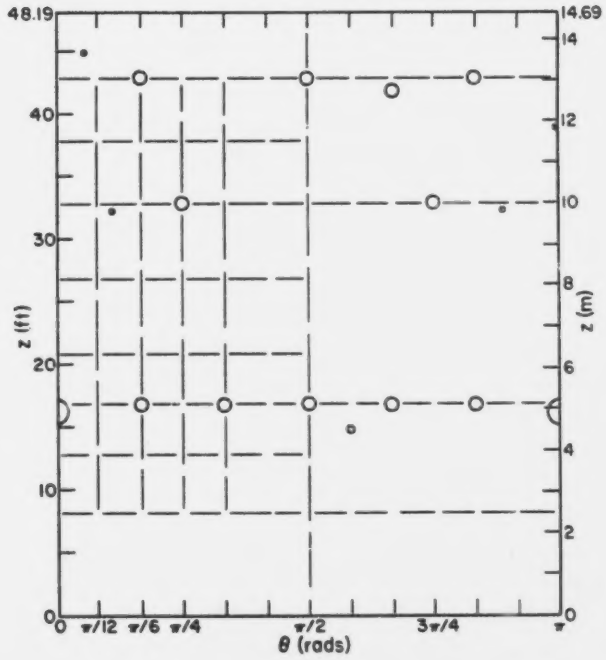

Fig. 12. Acceptable consolidation (42 annulus nodes). This figure also appears in Appendix B as Fig. B-1e.

and Fig. 3. Differences between the similar geometries are the number of auxiliary feedwater pipes, the annulus width, and the ratio of the break-node to annulus flow area to the break-node to drywell flow area. Therefore, Appendix C investigates the effect of noding consolidation for these different geometries by comparing the SSW loads for the base-case noding (Fig. 2) with the loads for the acceptable consolidation noding (Fig. 12, Case 5). This was done for (1) the base-case geometry annulus thickness decreased by 25 per cent, (2) the number of auxiliary feedwater pipes reduced from six to four, and (3) the ratio of the break-node to annulus outflow area relative to the break-node to drywell outflow area varied from the base-case value of 0.11 to 1.0.

It was found that the SSW maximum loads, the time of occurrence of the peak loads, and the variation of loads with time were insensitive to the noding consolidation for the different geometries studied. As a result, it appears that results of sensitivity studies based on the base case BWR cavity geometry are applicable to other similar geometries.

It should be noted that there are BWR cavity geometries, such as the General Electric Mark III, that are very different from the basic geometry studied.

B. Heat Transfer

We followed the subcompartment-analysis convention of ignoring heat transfer.

C. Blowdown

Subcompartment-analysis blowdown provides the driving potential for the calculated pressures. Blowdown is usually input to codes in the form of a mass-flow addition rate and corresponding enthalpy or energy addition rate as a function of time. Maximum calculated loads would logically result from maximum addition rates.

The node or nodes selected for the introduction of blowdown (break node or nodes) can have a significant effect on the calculated results. In particular, a blowdown jet or delayed liquid vaporization may cause a different mass and energy distribution than calculated by addition of the blowdown to only the break node(s),

with subsequent mass and energy distribution downstream of the break node(s) being determined from nodal pressure buildup and the code flow equations. As a result, the distribution might be reduced by the break-node(s) junctions, especially if flow between nodes is limited by the establishment of critical flow.

Calculated loads can be very sensitive to the rate of increase (ramp time) of the mass and energy addition rates. This is shown in Table E-II of Ref. 1. This effect is more important for calculated loads that occur within or near times that are affected by the possible ramp-time variation.

The blowdown for the BWR cavity studied in this report is introduced into a break node located in the SSW opening provided for the recirculation pipe, because this is where the safe-end weld is located (see Fig. 1c). As a result, the partitioning of the break flow between that going to the annulus and that going to the drywell is determined by the code.

Another possible way to determine the break-flow partitioning would be to determine the flow resistances from the break node for each of these paths. The break flow would then be partitioned accordingly. For example, if the resistance for flow to the annulus was twice the resistance for flow to the drywell, one-third of the break flow would be introduced to the annulus.

This approach, however, is less thorough than allowing the code to calculate the partitioning. The code would account for (1) mass storage in the break node and (2) variable flow resistance because of different densities along the two flow paths, a factor only important when the flow is subcritical. In Appendix C, Table C-III presents the results of varying the ratio of the area for flow from the break node to the annulus relative to the area for flow from the break node to the drywell.

Table D-I presents the effect on SSW loads of variation of the Moody critical flow multiplier. A particularly interesting result of this study is that the maximum loads were obtained when a Moody multiplier of 1.0 was used for the flow junctions from the break node along with a Moody multiplier of 0.6 for all other junctions. This is because the Moody multiplier of 1.0 provides increased mass and energy flow to the annulus, which results in higher SSW loads. One could better appreciate this result by considering the break node inside the SSW as an extension of the broken pipe for which break-flow rates are usually maximized to be conservative.

The above considerations indicate that conservatively high SSW loads will be obtained for geometries with breaks in the SSW by use of a Moody multiplier of 1.0 at the junctions from the break node and a Moody multiplier of 0.6 for all other junctions. However, the SSW loads for geometries with breaks in the annulus should be calculated with a Moody multiplier of 0.6 for all junctions, including those from the break node.

D. Initial Conditions

We believe that SSW loads are insensitive to minor variations of initial conditions (that is, pressure, temperature, humidity) based on the PWR study of these effects.[1] Therefore, a study of these effects was not included in this report.

E. Flow Modeling

The flow-modeling considerations discussed in this section generally parallel the US NRC guideline.[2] In addition, we have expanded on these guidelines based on our sensitivity studies.

1. Air Accounting. The significance of accounting for the initial presence of air instead of the all-steam approximation used by RELAP3[5] was studied in Ref. 1. Therefore, this matter will be deferred to the Ref. 1 results, which show that the x-force and y-moment were insensitive to the all-steam approximation.

2. Inertial Representation. Table D-II shows that calculated loads can be sensitive to the inertial representation.

Inertial representation is conventionally done by means of summing (L/A) terms. (L/A) is an expression for the integrated flow-path length to area ratio of a subcompartment. It is the length of the flow path from the node junction to the centroid of the node divided by the area of the node in the direction of flow. These terms are summed from node centroid to node centroid. The development of the (L/A) terms for flow

between nodes of different coarseness requires some care. For example, as shown in Fig. 13, the area of the coarse node (k) must be apportioned between the junctions 1 and 2. The apportionment actually depends on the node k flow area required for each of the junctions.

3. Compressibility. Compressibility can affect several features of subcompartment analysis including the (1) flow-path density, (2) vena contracta, and (3) loss coefficients. The flow-path density is in the equations used to calculate flow between nodes whereas the vena contracta affects entrance loss and orifice-discharge coefficients. Compressibility also affects exit-loss coefficients (see Ref. 8). There are several mitigating considerations that reduce the general influence of compressibility. These considerations are (1) compressibility usually affects a fraction of the total problem, that is, the high-velocity regions, (2) the high-velocity regions usually reach critical flow conditions and, therefore, critical flow models, which account for compressiblity, are used, (3) large flow-path density variations can often be accounted for by refined noding, and (4) some accounting for compressibility (that is, compressible nozzle equations) is usually incorporated in the codes used.[3,4] Analysis situations where these mitigating considerations mentioned above are not sufficient to reduce the impact of compressibility may warrant a more thorough accounting of compressibility.

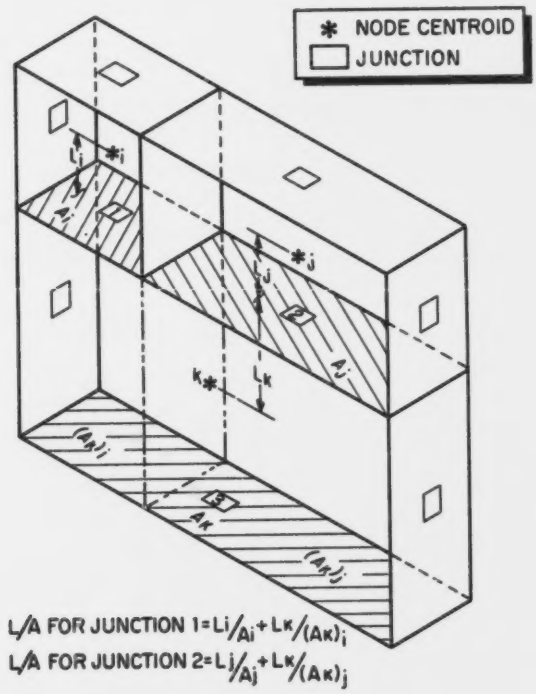

Fig. 13. Graphic representation showing three nodes of different coarseness and derivation of L/A terms.

4. Critical Flow Models. The US NRC recommends the use of the 0.6 Moody critical flow model.[2] In addition, the influence of the critical flow model may be complicated by problem geometry and thermodynamic condition.

In our reactor-cavity analyses for the BWR geometry studied, we found that only the flow junctions adjacent to the break node were critical (see Fig. 1c). All junctions in the reactor-cavity annulus were subcritical. As a result, variation of the critical flow model would affect primarily the flow rates from the break node.
break node.

Appendix D presents the effect of varying the noding and the critical flow model on SSW loads. This study shows that the conclusions made in Sec. IV.A.2 regarding the effect of noding consolidation are not affected by the critical flow model used. However, this study showed that the SSW loads can be very sensitive to variation in the Moody multiplier. This was caused by the increased Moody multiplier resulting in increased flow to the annulus through the critical flow junction from the break node. Of particular interest are the loads when a Moody multiplier of 1.0 is used for the junctions from the break node and a Moody multiplier of 0.6 is used elsewhere.

F. Flow Area

Flow area specification should be based on the minimum flow-path area between nodes. This is important because critical flow models (for example, HEM, Moody) are based on the minimum (throat) area, as are the head-loss coefficients.

Insulation Blockage. Flow area may vary with time because of the movement of seals and insulation. In particular, insulation displacement and

distribution might result in the blockage of some flow paths and affect the calculated results. A sophisticated mechanistic analysis would be required to estimate the history of insulation movement. Insulation causing blockage near the break would be exposed to higher pressure loads and, therefore, would be more likely to be displaced. This is a complicated problem requiring further investigation.

G. Loss Coefficients

Head-loss coefficients are conventionally used to account for total pressure losses caused by expansion. The SSW loads were found to be insensitive to loss-coefficient variation. Other problem geometries, initial conditions, and blowdowns might have different sensitivities. The main purpose of the following discussion is to normalize loss-coefficient determination, application, and reporting according to what might be considered "good practice." Subcompartment loss-coefficient modeling should thereby become a routine matter.

1. Sources. Many sources of loss-coefficient information exist, with Ref. 9 having great diversity. These sources use a coefficient to be multiplied by a reference velocity head, usually at the minimum flow area, to give the loss in total pressure caused by the geometric flow area variation being modeled. The flow is usually assumed to be incompressible.

2. Flow Direction Effect. Loss coefficients for a given geometry may depend on the direction of flow. This should be recognized in the determination of loss coefficient. For example, consider the loss coefficient for the junction between a large node i to a small node j. If the modeler assumed flow was from i to j, a total head-loss coefficient of about 0.5 might be used. However, flow from j to i might call for a total head-loss coefficient of about 1.0. Both loss coefficients would be applied to the same minimum flow area velocity head. As a result, the problem loss-coefficient specification must acknowledge the actual flow direction. Variation of flow direction during the calculation may not be important. However, this depends on the problem under analysis and the result of interest. The subcompartment-analysis code could automatically account for the loss-coefficient directional dependence, with loss coefficients for both directions specified (see Refs. 3 and 4).

3. Area Ratio Multipliers. It may be convenient to represent a flow loss by a flow area different from the flow area upon which the loss coefficient is based. An area ratio multiplier adjustment of the loss coefficient is therefore necessary to account for the difference in velocity heads. For example, consider the use of a junction area (A_A) different from the loss-coefficient basis area (A_B). The code input loss coefficient will be that based on A_B multiplied by (A_A/A_B) squared.

4. Node-to-Junction Representation. Separation of the losses being modeled into those between the junction and adjacent nodes is recommended so that the loss-coefficient distribution may be recognized. Codes that utilize the compressible nozzle equation (for example, Refs. 3 and 4) expect this type of breakdown. In addition, calculation of critical flow with an accounting for losses should only be based on the losses from the upstream node to the junction throat.

5. Compressibility. The effect of compressibility on loss coefficients has been investigated for simple geometries (see Ref. 8). However, the sensitivity study of Appendix D indicates that the SSW loads are insensitive to a $\pm$ 30 per cent variation of loss coefficients. Based on Ref. 8, it appears that the effect of compressibility on loss coefficients would result in a variation in this range, depending, of course, on the flow conditions and geometry. As a result, the use of incompressible loss coefficients, as is current practice, is probably acceptable for subcompartments we have studied. There certainly could be some analyses that require compressibility accounting, for example, an analysis dominated by compressible flow restrictions. The addition of such a capability is recommended for the future.

6. Detailing of Junction Loss-Coefficient Components. A detailed description of the component contribution to junction loss

coefficients is recommended to facilitate model evaluation and minimize the opportunity for errors. Appendix I of Ref. 1 presents an example of such a description. This example displays recognition of the flow direction, area ratio multiplier, and node-to-junction component representation.

H. Force-Moment Determination

1. General. The calculation of forces and moments that result from pressure distributions on a subcompartment component, that is, the SSW, requires several considerations. Included are a suitable coordinate system, the use of curved surface projected area for conversion of pressure to force, and the location of force-moment determination.

A right-hand coordinate system (usually Cartesian) should be used. As a result, the calculated forces and moments are more readily interpreted, communicated, and transposed to other right-hand coordinate systems. A Cartesian right-hand coordinate system can be described as follows. Rotation from the +x-axis toward the +y-axis results in advancement of a right-handed screw in the +z-direction. For example, reactor-cavity analyses discussed in this report have the +z-axis in the upward vertical direction through the SSW centerline, and the +x- and +y-axes are in the same plane as the bottom of the SSW (that is, z = o). This coordinate system has been chosen because moments tending to tip the SSW were assumed to be important for these analyses. In general, the location of the coordinate system should be located to produce force-moment results of greatest relevance. Note that for geometrically symmetrical problems, one of the coordinate axes can often be located to simplify the results by the elimination of some of the force-moment components.

The moments are determined from the x-, y-, and z-forces in conjunction with their moment arms between their lines of action and the axes about which they act. The signs of the moments are determined by the cross-product of the moment arm vector times the force vector. The moment arm vector is defined as the perpendicular vector distance from the moment axis to the line of action of the force vector. The moment is readily determined by using the right-hand rule.

The conversion of pressure acting on the curved surface to a force vector is facilitated by use of the projected planar area of the curved surface. Multiplication of the projected area by the pressure gives the net force vector magnitude with the vector line of direction acting normal to the projected area surface through its area centroid. Note that the net force acting on a curved surface will act through the surface center of revolution, which simplifies moment arm determination.

2. Nozzle and Piping Considerations. Component loading is affected by component appendages such as pressure vessel nozzles and piping. The SSW loads could be sensitive to appendage loading if the appendage (a) pressure difference is large, (b) force bearing area is a significant fraction of that for the component, or (c) involves a large moment arm. These considerations are quite problem specific. As a result, nozzle and piping effects must be evaluated for each analysis.

An obvious way to determine the effects of nozzles and piping is to include noding detail around the appendages and to then determine the appropriate loading. However, subcompartment analyses that include the necessary pressure distribution noding detail could be used to estimate the significance of the appendage loading from the pressure distribution only. As a result, the need to more thoroughly calculate the resulting loading might be eliminated.

REFERENCES

1. R. G. Gido, J. S. Gilbert, and C. G. Tinkler, "Subcompartment Analysis Procedures," Los Alamos Scientific Laboratory report LA-8169-MS (December 1979).

2. "Standard Review Plan for the Review of Safety Analysis Reports for Nuclear Power Plants," Section 6.2.1.2, Office of Nuclear Reactor Regulation, US Nuclear Regulatory Commission report NUREG-75/087, LWR edition (May 1980).

3. R. G. Gido, J. S. Gilbert, R. G. Lawton, and W. L. Jensen, "COMPARE-MOD 1: A Code for the Transient Analysis of Volumes with Heat Sinks, Flowing Vents, and Doors," Los Alamos Scientific Laboratory report LA-7199-MS (March 1978).

4. R. G. Gido, G. J. E. Willcutt, Jr., J. L. Lunsford, and J. S. Gilbert, "COMPARE-MOD 1 Code Addendum," Los Alamos Scientific Laboratory report LA-7199-MS, Addendum (NUREG/CR-1185 Addendum 1) (June 1980).

5. W. H. Retting, G. A. Jayne, K. V. Moore, C. E. Slater, and M. L. Uptmoor, "RELAP3 - A Computer Program for Reactor Blowdown Analysis," Idaho Nuclear Corporation report IN-1321 (June 1970).

6. R. A. Wells, "BEACON/MOD2A: A Computer Program for Subcompartment Analysis of Nuclear Reactor Containment," EG&G Idaho, Inc. report CDAP-TR-051 (March 1979).

7. A. Koestel, R. G. Gido, and J. S. Gilbert, "Film Entrainment and Deposition for Two-Phase Flow," Los Alamos Scientific Laboratory report LA-8475-MS (NUREG/CR-1634) (August 1980).

*8. J. F. Jackson and M. G. Stevenson, "Nuclear Reactor Safety Progress Report, July 1 - September 30, 1978," Los Alamos Scientific Laboratory report LA-7567-PR (NUREG/CR-0522) December 1978.

9. I. E. Idel'chik, "Handbook of Hydraulic Resistance," US Department of Commerce, National Bureau of Standards, Institute for Applied Technology, US Atomic Energy Commission report AEC-tr-6630 (1966).

* A more complete description of this work will be published by A. Koestel and R. G. Gido, "Compressibility Effects on Containment Subcompartment Loss Coefficients," Los Alamos National Laboratory report.

APPENDIX A

APPLICATION OF GENERAL NODING PROCEDURES TO REPRESENTATIVE BWR CAVITY

The purpose of this appendix is to apply the general procedures for noding described in Sec. IV.A.1 to the BWR cavity studied, which is described in Figs. 1a - 1c. Figure A-1 represents this geometry by "unwrapping" the reactor-cavity annulus on a plane of height vs the distance around the circumference (in radians). Figure A-2 shows the noding that results from application of the general procedures. This noding forms the base case for the noding consolidation study presented in Appendix B and other comparisons.

Major annulus geometric features are shown in Fig. A-1. In particular, note that the width of the annular gap between the SSW and the insulation is 0.122 m (0.4 ft) above a z-elevation of ~ 2.5 m (~ 8 ft) and 0.546 m (1.792 ft) below this height. Figure A-1 and Table A-I describe the obstructions that are created by the pipes going from the reactor pressure vessel through the SSW. In particular, note the rows of pipes at (1) a z-elevation of ~ 5.1 m (~ 16.7 ft) that include the 0.61 m (24 in) diameter recirculation lines at 0 and π radians, and (2) a z-elevation of ~ 13 m (43 ft), around which there is flow from the annulus to the drywell. Of less importance are the row of pipes at a z-elevation of ~ 10 m (33 ft) and the small pipes through the annulus at irregular intervals.

Application of the general procedures for noding results in the Fig. A-2 noding. Particular features to be noted are:

(1) Problem symmetry is utilized so that only 0 to π is modeled.

(2) The break is located at 0 rad and 4.8 m (15.75 ft).

(3) A vertical string of junctions is located at $\pi/2$ rad.

(4) Horizontal strings of junctions are located where there are horizontal rows of pipes.

(5) A horizontal string of junctions is located where the annulus width changes.

(6) A string of junctions in the vertical and horizontal direction passes through all major pipe obstructions. However, a few pipes required slight movement to satisfy this requirement.

(7) Noding is finer near the break.

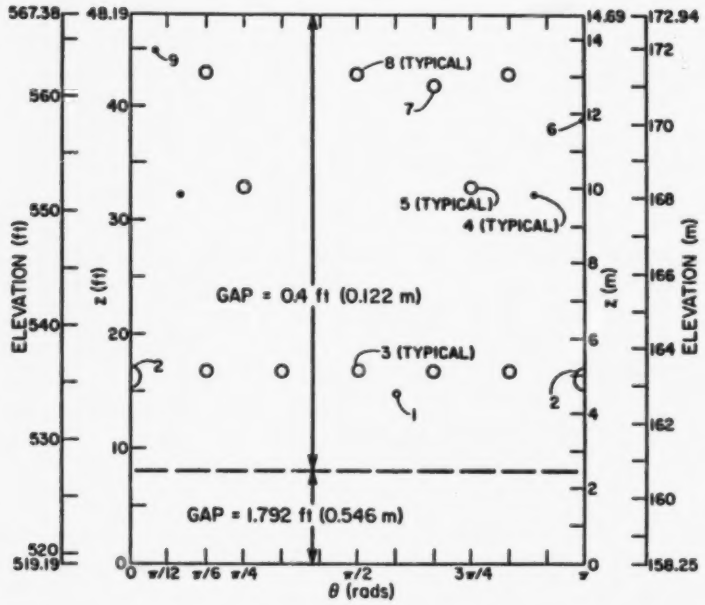

Fig. A-1. This is the "unwrapped" BWR cavity that was studied in this report showing pipe (see Table A-I) locations in the symmetric 0 to π rad model used for calculations. Also shown are the elevation from the SSW bottom (z = 0) and the annulus gap (between the SSW and insulation) variation. Blowdown is introduced at the recirculation outlet pipe located at 0 rad and z ≅ 5 m (~ 16 ft). There is exit flow from the annulus top around the stabilizers and through the SSW penetrations associated with the core spray (7) and the feedwater pipes (8). This figure is also shown in the text as Fig. 3.

(8) Arbitrary strings of junctions are positioned to avoid large nodes surrounded by smaller nodes.

Appendix B shows that the SSW loads are approximately insensitive to the noding consolidation of the Fig. A-2 noding (72 annulus nodes) to the Fig. B-1e noding (42 annulus nodes). Sensitivity studies are performed in other appendixes using this consolidated noding.

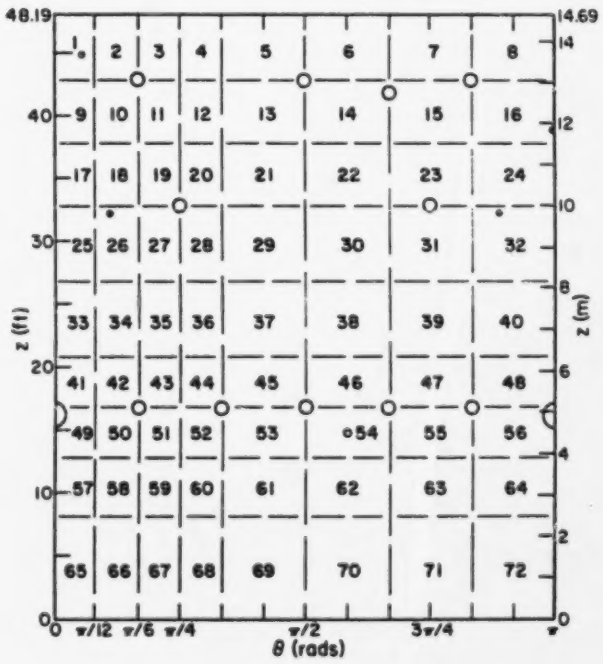

Fig. A-2. Noding of the BWR cavity described in Fig. A-1 based upon the procedures described in Sec. IV.A.1. This figure is also shown in the text as Fig. 2.

TABLE A-I

DESCRIPTION OF SSW PIPE PENETRATIONS SHOWN IN FIG. A-1

Identification Number on Fig. A-1	Number of pipes over full 0 to 2π rad circumference[a]	Diameter on Fig. A-1 m	Diameter on Fig. A-1 (in)	Description[b]
1	2	.102	(04)	Jet pump instrumentation
2	2	.610	(24)	Recirculation outlet
3	10	.305	(12)	Recirculation inlet
4	4	.051	(02)	Instrumentation water level
5	4	.305	(12)	RHR/LPCI
6	1	.076	(03)	CRD H_2 system
7	2	.254	(10)	Core spray (LP, HP)
8	6	.305	(12)	Feedwater
9	2	.051	(02)	Instrumentation water level

[a]The 0 to π rad model shown in Fig. A-1 has one-half as many pipes.
[b]RHR = Residual Heat Removal
LPCI = Low Pressure Coolant Injection
CRD = Control Rod Drive
LP = Low Pressure
HP = High Pressure

APPENDIX B

EFFECT OF BWR CAVITY NODE CONSOLIDATION ON SACRIFICIAL SHIELD-WALL FORCES AND MOMENTS

The object of this appendix is to get some idea of the fineness of noding required in areas where there is uncertainty as to the fineness needed.

The base-case noding used as a starting point is that developed in Appendix A and is based on the general procedures for noding described in Sec. IV.A.1, see Fig. 2. Table B-I summarizes the results of the progressive consolidations with all previous case consolidations retained. For example, Fig. B-1e shows the acceptable consolidated model used for sensitivity studies with only 42 annulus nodes, whereas the base case has 72 annulus nodes.

The consolidation follows the general procedures for noding set forth in Sec. IV.A.1. In particular, the junctions along π/2 rad, along the step in the annulus thickness, and along the rows of pipes were left intact throughout. The other junctions were progressively consolidated towards the break.

Figures B-1a through B-1g and Table B-I illustrate the progress of the consolidations. Some of the consolidations we performed are not shown in these figures because they were superfluous. As expected, SSW loads were insensitive to consolidations far from the break. Relatively extensive consolidations between π/2 and π rad resulted in changes in force and moment of less than approximately 2 per cent. However, fairly minor consolidations near the break and along the upper row of pipes between 0 and π/2 rad had sharper effects because of the steeper pressure gradient nearer the break. It is interesting to note that none of our models, even Case 7, had forces and moments more than 11 per cent different from the base case. Had the criteria for "insensitive" been ± 11 per cent, rather than the ± 5 per cent used in the PWR study, one could have called all of our models "insensitive."

One goal of this consolidation exercise was to develop an "acceptable consolidation." This

TABLE B-I

EFFECT OF NODE CONSOLIDATION ON BWR SSW MAXIMUM FORCE (F_x) AND MOMENT (M_y)

Case	Number of Annulus Nodes	% Difference Relative to Base Case		Corresponding Figure
		F_x	M_y	
Base	72	-	-	A-2
1	68	0	0	B-1a
2	60	+1	-3	B-1b
3	50	+2	-2	B-1c
4	46	+2	-2	B-1d
5[a]	42	-2(-4)	-2(-7)	B-1e
6	30	-4	-6	B-1f
7	18	-5(-5)	-6(-11)	B-1g

Notes:

1. Times of occurrence of the values compared are approximately the same.

2. Base case values and times of occurrence are:

   F_x = 12.50 MN (2.81 x 10^6 lb_f) at .0245 s
   M_y = 77.1 MN-m (6.79 x 10^8 lb_f-in) at .0245 s.

3. The per cent differences in parentheses are those obtained with the junction areas from the break node (that is, to the annulus and drywell) reduced by 50 per cent. The resulting base case values and times of occurence are:

   F_x = 5.92 MN (1.33 x 10^6 lb_f) at .0255
   M_y = 39.0 MN-m (3.45 x 10^8 lb_f-in) at 0.255.

[a]Acceptable consolidation noding used for other studies in this report.

was chosen from our models on the basis of (1) approximately meeting the "insensitive" criterion mentioned above and (2) being easily adaptable to other similar reactor cavity geometries by following the general noding procedures of Sec. IV.A.1, that is, the large nodes are defined by junctions that satisfy the procedures. Case 5 was chosen as the model that most closely met these requirements. The 7 per cent difference in maximum y-moment was considered to be insignificantly different from the arbitrary 5 per cent insensitive criterion. This acceptable consolidation was used for the sensitivity studies presented in other appendixes.

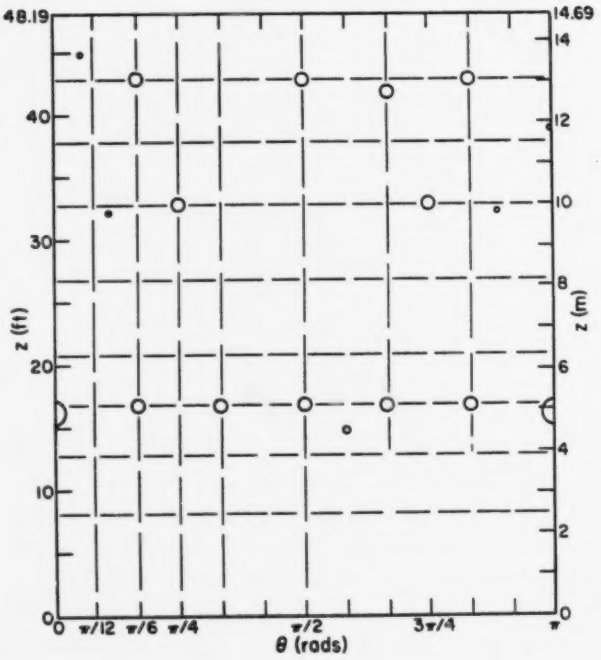

Fig. B-1a. Case 1 (68 annulus nodes)

Fig. B-1. Progressive consolidated noding of the base-case noding shown in Fig. A-2 with 72 annulus nodes. See Table B-1 for the effect of noding consolidation on SSW loading. Note that Case 5 is the "acceptable" consolidation noding used in other studies in this report. Figure B-1e is also shown in the text as Fig. 12.

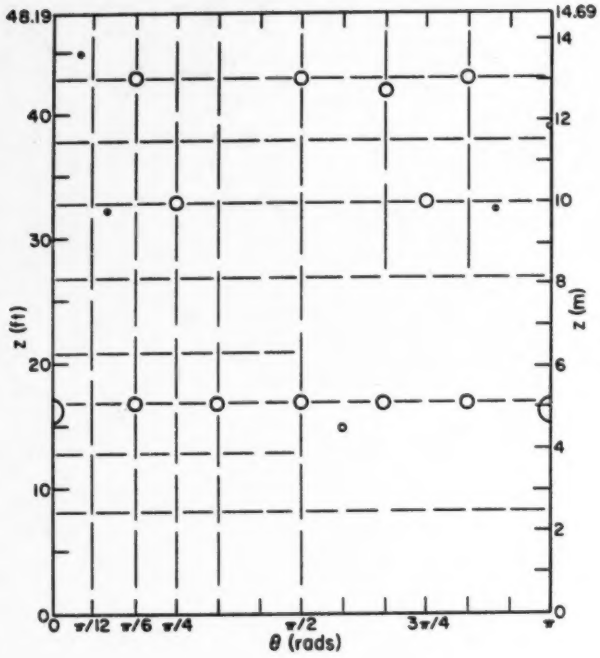

Fig. B-1b. Case 2 (60 annulus nodes)

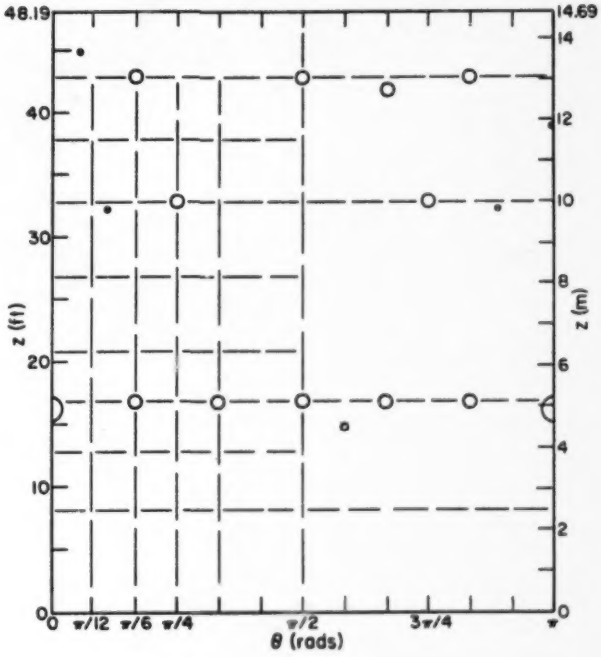

Fig. B-1d. Case 4 (46 annulus nodes)

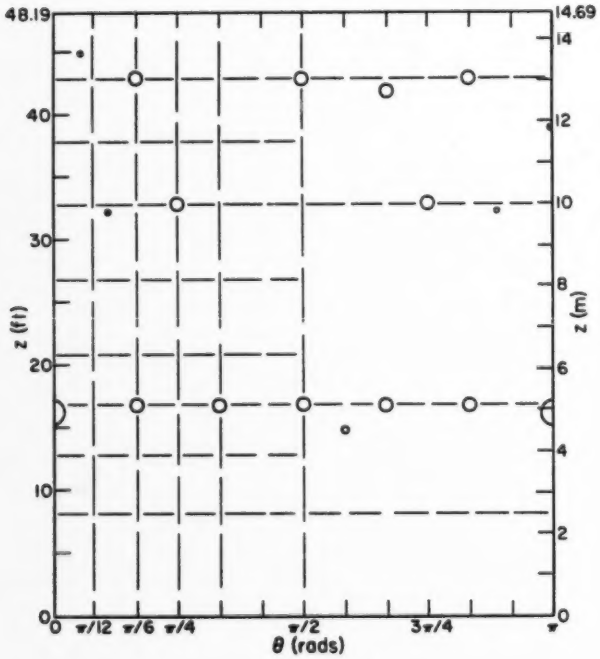

Fig. B-1c. Case 3 (50 annulus nodes)

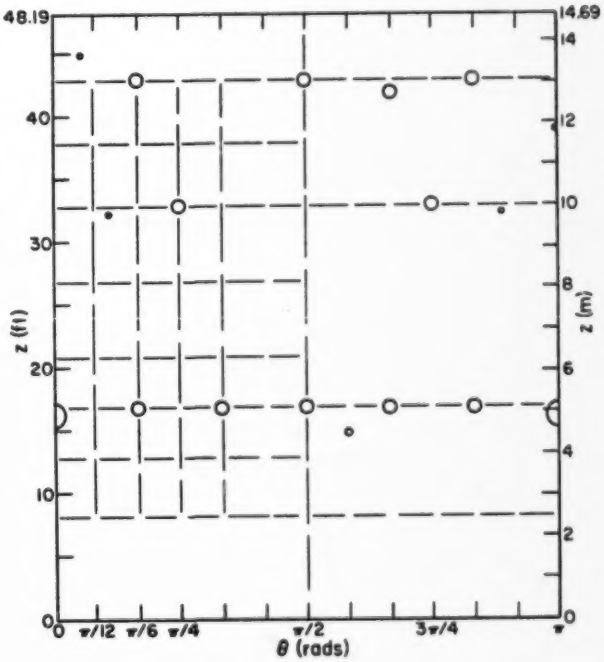

Fig. B-1e. Case 5 (42 annulus nodes)*

Fig. B-1 Continued

*This figure also appears in the text as Fig. 12.

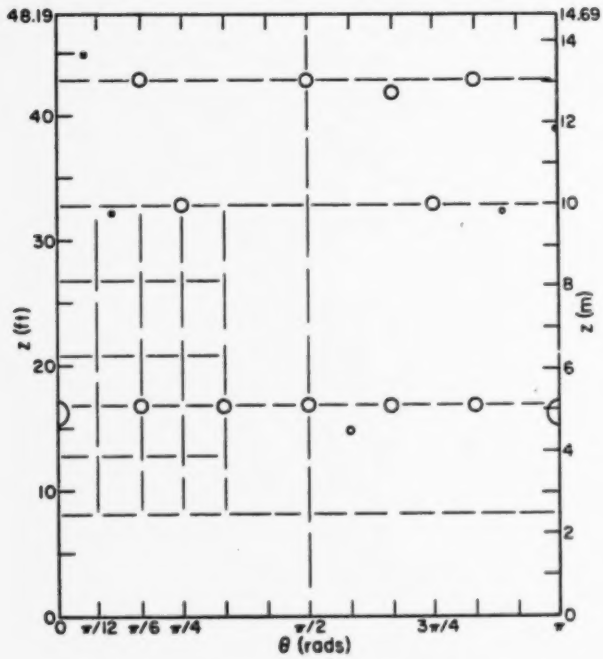

Fig. B-1f. Case 6 (30 annulus nodes)

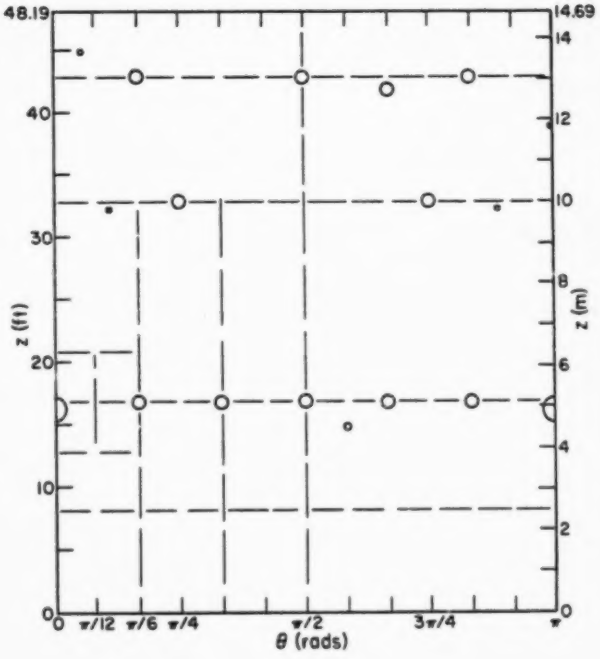

Fig. B-1g. Case 7 (18 annulus nodes)

Fig. B-1 Continued.

APPENDIX C

EFFECT OF NODE CONSOLIDATION FOR OTHER BWR CAVITY GEOMETRIES

The BWR cavity depicted in Figs. 1a - 1c was used for our sensitivity studies. Two other BWR cavities of similar geometry were studied and found to be only slightly different from our geometry. Primary differences were found to be in the width of the annulus, the number of auxiliary feedwater pipes, and the relative flow area from the break node to the reactor-cavity annulus in comparison to the flow area to the drywell. The purpose of this appendix is to investigate the effect of the noding consolidation developed in Appendix B for these different geometries.

Note that there are BWR cavity geometries that are much different from those studied in this report.

Table C-I shows that the Case 5 (Fig. B-1e) noding represents an acceptable consolidation relative to the base-case noding (Fig. A-2) for the reduced annulus width. Note, however, that reducing the annulus width increases the x-force and y-moment on the SSW.

Table C-II shows that the Case 5 noding also represents an acceptable consolidation relative to the base-case noding for four and six auxiliary feedwater pipes. Note the small increase in SSW force and moment associated with this variation.

Table C-III shows that the Case 5 noding is still an acceptable alternative to the base-case noding for different values for the break-node outflow area ratio. Table C-III shows the

TABLE C-I

EFFECT OF NODE CONSOLIDATION ON MAXIMUM SSW FORCES AND MOMENTS FOR DIFFERENT ANNULUS WIDTHS

MAXIMUM X-FORCE, MN (10^6 lb_f)

Annulus Width	Base-Case Noding Fig. A-2	Case 5 Noding Fig. B-1e	% Difference
Base Case Geometry Width	12.5 (2.82)	12.3 (2.76)	-2
75% of Base Case Geometry Width	16.2 (3.65)	15.6 (3.51)	-4

MAXIMUM Y-MOMENT MN-m (10^8 lb_f-in)

Annulus Width	Base-Case Noding Fig. A-2	Case 5 Noding Fig. B-1e	% Difference
Base Case Geometry Width	77.1 (6.79)	75.2 (6.62)	-2
75% of Base Case Geometry Width	95.3 (8.43)	92.5 (8.18)	-3

TABLE C-II

EFFECT OF NODE CONSOLIDATION ON MAXIMUM SSW FORCES AND MOMENTS FOR DIFFERENT NUMBERS OF FEEDWATER PIPES

MAXIMUM X-FORCE MN (10^6 lb_f)

Number of Feedwater Pipes	Base-Case Noding	Case 5 Noding	% Difference
Six	12.54 (2.82)	12.28 (2.76)	-2
Four	13.08 (2.94)	12.59 (2.83)	-4

MAXIMUM Y-MOMENT MN-m (10^8 lb_f-in)

Number of Feedwater Pipes	Base-Case Noding	Case 5 Noding	% Difference
Six	77.1 (6.79)	75.2 (6.62)	-2
Four	84.6 (7.48)	80.4 (7.12)	-5

TABLE C-III

EFFECT OF CHANGING BREAK-NODE OUTFLOW AREA RATIO

MAXIMUM X-FORCE MN (10^6 lb_f)

Area Ratio[a]	Base-Case Noding[b]	Case 5 Noding[c]	% Difference[d]
0.11	12.50 (02.82)	12.30 (02.76)	-2
0.34	38.17 (08.58)	35.81 (08.05)	-6
0.56	59.43 (13.36)	55.56 (12.49)	-6
0.78	74.82 (16.82)	67.52 (15.81)	-6
1.00	76.15 (17.12)	80.07 (18.00)	-6

MAXIMUM Y-MOMENT MN-m (10^8 lb_f-in)

Area Ratio[a]	Base-Case Noding[b]	Case 5 Noding[c]	% Difference[d]
0.11	77.1 (6.79)	75.2 (6.62)	-2
0.34	233.0 (20.5)	218.0 (19.2)	-6
0.56	365.8 (32.3)	344.6 (30.4)	-6
0.78	461.6 (40.7)	436.0 (38.5)	-6
1.00	523.2 (46.2)	494.6 (43.6)	-5

[a] Area Ratio is the ratio of the break node to annulus outflow area to the break node to drywell outflow area.

[b] See Fig. A.2.

[c] Determined to be an acceptable consolidation in Appendix B, see Fig. B-1e.

[d] Case 5 vs. Base-Case noding.

results of progressively increasing the outflow area from the break node to the annulus, until it is the same as the outflow area from the break node to the drywell (see Fig. 1c). Note that the peak forces and moments in the annulus increase approximately linearly with respect to the area ratio except for the high ratios. The difference betweeen the base case and Case 5 in both force and moment is close to a constant 6 per cent.

Indications are that the mass-flow rate ratio for flows out of the break node is identical to the outflow area ratio, and that this mass-flow rate ratio is also constant (within $\pm$ 3 per cent) with respect to time (see Table C-IV). This is in contrast to the ratio of <u>total</u> break mass-flow rate to annulus mass-flow rate. This ratio changes very significantly with respect to time because mass is stored in the break node and the total blowdown rate is constant for the time intervals we are considering ($t < 1$ s).

TABLE C-IV

MASS-FLOW RATES AND MASS-FLOW RATIOS AS A FUNCTION OF TIME

A. BASE CASE WITH ORIGINAL AREA RATIO OF .11

Time, s	Mass-Flow Rate, kg/s To Annulus	Mass-Flow Rate, kg/s To Drywell	Mass-Flow Rate Ratio Annulus/Drywell
.00002	16.0	150.0	.11
.00004	23.7	222.0	.11
.001	282.0	2637.6	.11
.005	688.3	6436.5	.11
.010	865.5	8094.8	.11
.015	951.8	8900.8	.11
.020	1006.3	9409.8	.11
.025	1045.3	9774.5	.11
.030	1075.1	10053.0	.11

B. BASE CASE WITH AREA RATIO OF 1.00

Time,s	Mass-Flow Rate, kg/s To Annulus	Mass-Flow Rate, kg/s To Drywell	Mass-Flow Rate Ratio Annulus/Drywell
.00002	1500	1500	1.00
.00004	2212	2212	1.00
.001	2435	2435	1.00
.005	5325	5325	1.00
.010	6257	6260	1.00
.015	6617	6650	1.00
.020	6765	6857	0.99
.025	6825	6973	0.98
.030	6840	7042	0.97

C. BASE CASE WITH ORIGINAL AREA RATIO OF .11
TOTAL BREAK FLOW

Time, s	Mass-Flow Rate, kg/s Total Break	Mass-Flow Rate, kg/s To Annulus	Mass-Flow Rate Ratio Total/Drywell
.00002	14081	16.0	880
.00004	14081	23.7	594
.001	14081	282.0	49.9
.005	14081	688.3	20.5
.010	14081	865.5	16.3
.015	14081	951.8	14.8
.020	14081	1006.3	14.0
.025	14081	1045.3	13.5
.030	14081	1075.1	13.1

APPENDIX D

SENSITIVITY STUDIES

The purpose of this appendix is to present the results of various sensitivity studies that were performed with our "acceptable consolidation" noding shown in Fig. B-1e (Case 5).

Table D-I shows the effect on SSW loads of varying the noding and the critical flow model used. The loads are shown to be insensitive to the noding variation. However, the loads are sensitive to variation of the critical flow models.

The Best Estimate Values (BEV) for the inertia term were modified by a factor of ± 30 per cent. Table D-II shows that the SSW forces and moments are sensitive to changes in this parameter.

BEV for the entrance and exit loss coefficients were also modified by ± 30 per cent. The calculated forces and moments were insensitive to this variation (see Table D-III).

TABLE D-I

EFFECT OF CRITICAL FLOW MODEL AND NODING ON SSW LOADS

Notes: (1) The base-case noding has 72 annulus nodes (see Fig. A-2).
(2) The Case 5 noding has 42 annulus nodes (see Fig. B-1e).

	x-Force, MN (10^6 lb_f)				% Difference Between Base Case and Case 5
Critical Flow Model	Base Case		Case 5		
-1.0 Moody everywhere[a]	12.0	(2.69)	11.5	(2.58)	-2
0.6 Moody everywhere	12.5	(2.81)	12.3	(2.76)	-2
0.8 Moody everywhere	13.9	(3.12)	13.5	(3.03)	-3
1.0 Moody everywhere	14.8	(3.32)	14.3	(3.22)	-3
1.0 Moody for flow from the break node and 0.6 Moody elsewhere	21.1	(4.75)	20.2	(4.55)	-4

	y-Moment, MN-m (10^8 lb_f-in)				% Difference Between Base Case and Case 5
Critical Flow Model	Base Case		Case 5		
-1.0 Moody everywhere[a]	72.6	(06.40)	70.7	(06.23)	-3
0.6 Moody everywhere	77.1	(06.79)	75.2	(06.62)	-2
0.8 Moody everywhere	87.2	(07.68)	84.6	(07.45)	-3
1.0 Moody everywhere	92.9	(08.18)	90.2	(07.95)	-3
1.0 Moody for flow from the break node and 0.6 Moody elsewhere	126.0	(11.10)	122.5	(10.80)	-3

[a]In COMPARE, this results in the Homogeneous Equilibrium Critical Flow Model.

TABLE D-II

EFFECTS ON FORCES AND MOMENTS
OF VARYING INERTIA TERMS

Multiplier of BEV[a] L/A Term	% Change In X-Force	% Change In Y-Moment
0.7	-14	-16
1.0	---	---
1.3	+12	+14

[a]BEV - Best Estimate Value

TABLE D-III

EFFECTS ON FORCES AND MOMENTS OF VARYING
ENTRANCE AND EXIT LOSS

Multiplier of BEV[a] Entrance Losses	% Change In X-Force	% Change In Y-Moment
0.7	-0.1	-0.1
1.0	---	---
1.3	+0.1	+0.1

Multiplier of BEV[a] Entrance Losses	% Change In X-Force	% Change In Y-Moment
0.7	-0.1	-0.1
1.0	---	---
1.3	+0.1	+0.1

[a]BEV - Best Estimate Value

DISTRIBUTION

	Copies
Nuclear Regulatory Commission, R4, Bethesda, Maryland	298
Technical Information Center, Oak Ridge, Tennessee	2
Los Alamos National Laboratory, Los Alamos, New Mexico	50
	350

NRC FORM 335 (11-81)

U.S. NUCLEAR REGULATORY COMMISSION

BIBLIOGRAPHIC DATA SHEET

1. REPORT NUMBER *(Assigned by DDC)*
NUREG/CR-2633
LA-9277-MS

4. TITLE AND SUBTITLE *(Add Volume No., if appropriate)*
Containment Reactor Cavity Subcompartment Analysis Procedures for a Boiling Water Reactor

2. *(Leave blank)*

3. RECIPIENT'S ACCESSION NO.

7. AUTHOR(S)
W. V. Turk, R. G. Gido, C. Y. Li

5. DATE REPORT COMPLETED
MONTH February YEAR 1982

9. PERFORMING ORGANIZATION NAME AND MAILING ADDRESS *(Include Zip Code)*
Los Alamos National Laboratory
Los Alamos, NM 87545

DATE REPORT ISSUED
MONTH May YEAR 1982

6. *(Leave blank)*

8. *(Leave blank)*

12. SPONSORING ORGANIZATION NAME AND MAILING ADDRESS *(Include Zip Code)*
Division of Systems Integration
Office of Nuclear Reactor Regulation
U. S. Nuclear Regulatory Commission
Washington, D. C. 20555

10. PROJECT/TASK/WORK UNIT NO.

11. FIN NO.
A7119

13. TYPE OF REPORT
Technical

PERIOD COVERED *(Inclusive dates)*

15. SUPPLEMENTARY NOTES

14. *(Leave blank)*

16. ABSTRACT *(200 words or less)*

Procedures for the performance of Boiling Water Reactor (BWR) cavity subcompartment analysis are presented. The purpose of this presentation is to normalize the analysis procedures and to provide a standard approach for such analyses. As a result, differences in the manner of performing subcompartment analyses can be minimized and more readily understood and evaluated by others. The procedures were developed within the constraint of current code capability for the performance of such analyses and the current US Nuclear Regulatory Commission guidelines. A wide range of the effects of input and modeling variations on calculated sacrificial shield-wall (SSW) forces and moments were studied. The studies were for a representative BWR cavity geometry with the pipe break inside the SSW. The COMPARE subcompartment analysis code was used for the studies.

17. KEY WORDS AND DOCUMENT ANALYSIS

17a. DESCRIPTORS

BWR Reactor Cavity
Subcompartment Analysis

17b. IDENTIFIERS/OPEN-ENDED TERMS

18. AVAILABILITY STATEMENT
Unlimited

19. SECURITY CLASS *(This report)*
Unclassified

21. NO. OF PAGES

20. SECURITY CLASS *(This page)*
Unclassified

22. PRICE
$

NRC FORM 335 (11-81)